Technical Report Documentation Page

1. Report No. ABC-UTC-2016-C1-FIU 02	2. Government Accession No.	3. Recipient's Catalog No.	
4. Title and Subtitle Field Demonstration, Instrumentation, and Monitoring of Accelerated Repair Using UHPC Shell.		5. Report Date April 2021 6. Performing Organization Code	
7. Author(s) Alireza Valikhani and Kingsley Lau (https://orcid.org/0000-0003-0726-7667)		8. Performing Organization Report No.	
9. Performing Organization Name and Address Department of Civil and Environmental Engineering Florida International University 10555 West Flagler Street, EC 3680 Miami, FL 33174		10. Work Unit No. (TRAIS) 11. Contract or Grant No. 69A3551747121	
12. Sponsoring Organization Name and Address Accelerated Bridge Construction University Transportation Center Florida International University 10555 W. Flagler Street, EC 3680 Miami, FL 33174		13. Type of Report and Period Covered Final Report (March 2019- April 2021) 14. Sponsoring Agency Code	
15. Supplementary Notes Visit www.abc-utc.fiu.edu for other ABC reports.			
16. Abstract Highway bridge concrete structures subjected to marine environments are susceptible to chloride-induced corrosion. In part to address impacts on bridge service, accelerated bridge construction (ABC), have been introduced to minimize the impacts of construction on the community. ABC designs incorporating the application of ultra-high performance concrete (UHPC) on the retrofit of bridge substructure elements can locally minimize corrosion macrocell coupling and provide benefit above conventional patch repairs that are still used. Using a thin layer of the UHPC on the damaged areas as a protective shell can be an economical repair method to rehabilitate and protect bridge elements in severe environments. A large scale test beam was constructed and retrofitted with UHPC to identify corrosion macrocell coupling. Additional testing was made to address the effect of fibers on the electrical properties of UHPC. The electrical potentials of the rebar embedded in the chloride-free NC adjacent to corroding bars in chloride-rich concrete developed moderate potentials in the range of -0.2 to -0.4 VCSE. All of the rebar embedded in the UHPC developed passive potentials. The moderate potentials developed in the chloride-free NC concrete was related to the coupling of the actively corroding steel in the chloride-contaminated region. The results show that the presence of fibers have an effect to reduce the overall electrical resistivity and possibly oriented pathways in the cement microstructure along the fiber interface that can facilitate ionic movement. The results suggested that the parallel orientation of conductive fibers with the current path at high enough concentrations can create a system where electronic charge through the conductive fiber can be facilitated. Specimens with the steel fiber aligned orthogonal to the current path resulted in larger electrical resistance in comparison to when the steel fibers were aligned parallel with the current path. This effect was not observed for the specimens cast with fiberglass. Also, the overall electrical resistance was lower for the specimens cast with steel fibers than the less conductive fiberglass fibers. It was proposed that the presence of the conductive fibers can facilitate shorter paths for charged species to move in UHPC bulk by bridging ionic paths through the pores by electronic paths via the conductive fiber			
17. Key Words Repair, UHPC, Macrocell, Corrosion, Durability		18. Distribution Statement No restrictions.	
19. Security Classification (of this report) Unclassified.	20. Security Classification (of this page) Unclassified.	21. No. of Pages 49	22. Price

Form DOT F 1700.7 (8-72) Reproduction of completed page authorized

(this page is intentionally left blank)

Field Demonstration, Instrumentation, and Monitoring of Accelerated Repair Using UHPC Shell

Final Report

April 2021

Principal Investigator: Kingsley Lau
Department of Civil and Environmental Engineering
Florida International University

Authors
Alireza Valikhani and Kingsley Lau

Sponsored by
Accelerated Bridge Construction University Transportation Center

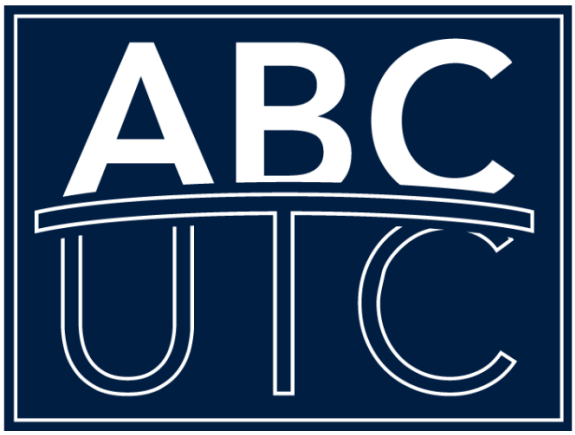

ACCELERATED BRIDGE CONSTRUCTION
UNIVERSITY TRANSPORTATION CENTER

A report from
Florida International University
Dept. of Civil and Environmental Engineering
10555 West Flagler Street
Miami, FL 33174
Phone: 305-348-2824 / Fax: 305-348-2802
https://cee.fiu.edu

DISCLAIMER

The contents of this report reflect the views of the authors, who are responsible for the facts and the accuracy of the information presented herein. This document is disseminated in the interest of information exchange. The report is funded, partially or entirely, by a grant from the U.S. Department of Transportation's University Transportation Program. However, the U.S. Government assumes no liability for the contents or use thereof.

ACKNOWLEDGEMENT

The assistance and support by the FIU ABC-UTC team and Dr. Atorod Azizinamini is much appreciated.

EXECUTIVE SUMMARY

Highway bridge concrete structures subjected to marine environments are susceptible to chloride-induced corrosion. In part to address impacts on bridge service, accelerated bridge construction (ABC), have been introduced to minimize the impacts of construction on the community. ABC designs incorporating the application of ultra-high performance concrete (UHPC) on the retrofit of bridge substructure elements have the benefit to strengthen existing bridge substructures as well as ideally to provide a durable substructure. UHPC in retrofit of corroded concrete can locally minimize corrosion macrocell coupling and provide benefit above conventional patch repairs that are still used. Further testing on the extent of macrocell coupling for various repair geometries utilized UHPC is warranted. Using a thin layer of the UHPC on the damaged areas as a protective shell can be an economical repair method to rehabilitate and protect bridge elements in severe environments as well as to increase the strength and performance of the bridge structure. A large scale test beam was constructed and retrofitted with UHPC to identify corrosion macrocell coupling. Additional testing was made to address the effect of fibers on the electrical properties of UHPC.

The steel embedded in the chloride contaminated region of the concrete T-beam developed highly electronegative potentials indicative of the expected corrosion activity. The electrical potentials of the rebar embedded in the chloride-free NC developed moderate potentials in the range of -0.2 to -0.4 V_{CSE} even though passive corrosion conditions was expected there. All of the rebar embedded in the UHPC developed passive potentials. The moderate potentials developed in the chloride-free NC concrete was related to the coupling of the actively corroding steel in the chloride-contaminated region. There can be significant polarization of the adjacent steel embedded in the rather poor quality concrete (lower resistivity). Conversely, this polarization did not occur for any of the steel rebar embedded in the UHPC (including those directly adjacent to the NC region. This observation highlights the effect of the high quality UHPC to minimize the extent of macrocell coupling of the anodes to the extended cathodes in the steel embedded in the shell repair.

At day 36, there was a clear linear relationship between the macrocell current and the cathode-to-anode ratio for the cathodes in the UHPC repair. The larger extended cathode in the UHPC allowed for larger macrocell currents to develop. The macrocell current was much larger when the cathode was the steel embedded in the concrete core substrate. Even though the embedded steel there would be encapsulated with the UHPC that could minimize oxygen transport, there would be sufficient oxygen in the substrate concrete pore water to support the cathodic oxygen reduction reaction.

The method of casting can have a significant influence on fiber distribution and orientation. Specimens with 2% steel fiber showed slightly higher resistance than samples with steel 4% fiber. The results show that the presence of fibers have an effect to reduce the overall electrical resistivity likely in part related to partial volume replacement of high quality cement and possibly oriented pathways in the cement microstructure along the fiber interface that can facilitate ionic movement. The results suggested that the parallel orientation of conductive fibers with the current path at high enough concentrations can create a system where electronic charge through the conductive fiber can be facilitated, and the lower electrical resistance can be better attributed to electronic charge motion rather than any preferred ionic motion that may develop at the fiber-cement interface. The orientation of the steel fibers have significant influence on the overall bulk UHPC resistance. Specimens with the steel fiber aligned orthogonal to the current path resulted in larger electrical resistance in comparison to when the steel fibers were aligned parallel with the current path. This effect was not observed for the specimens cast with fiberglass. Also, the overall electrical resistance was lower for the specimens cast with steel fibers than the less conductive fiberglass fibers.

It was proposed that the presence of the conductive fibers can facilitate shorter paths for charged species to move in UHPC bulk by bridging ionic paths through the pores by electronic paths via the conductive fiber.

TABLE OF CONTENTS

LIST OF TABLES

LIST OF FIGURES

1 INTRODUCTION

1.1 Background

Highway bridge concrete structures subjected to marine environments and de-icing salt applications are susceptible to chloride-induced corrosion. In those cases, the service life of the concrete structure is related to the permeability of the concrete and the design details for the reinforcing steel. Concrete with low water-to-cement ratio, high cement factors, and mix designs utilizing pozzolans (such as fly ash and silica fume) have low permeability and high concrete electrical resistivity that can resist the transport of chloride ions (that will allow depassivation of the steel) through the concrete cover and impede ionic coupling of corrosion macrocells. Reinforced concrete designs with details for larger rebar clear cover further extend the time to corrosion initiation. Other corrosion mitigation technologies include use of corrosion resistant reinforcing materials, corrosion inhibitors, application of cathodic protection, and coatings and sealers.

Despite the available corrosion mitigation technologies, degradation of reinforced concrete structures due to corrosion continue to be a major cost in bridge maintenance and repairs. Fifteen percent of US bridges are considered structurally deficient due to corrosion and the annual cost of corrosion of highway bridges exceed $8.3 billion [1]. The high cost of corrosion degradation of highway bridges in part relates to the expectation of extended bridge service life for older bridges built with less robust designs and materials for corrosion control and greater service expectations in terms of loads, design, and durability in aggressive exposure environmental. Furthermore, corrosion control measures are still needed for contemporary bridge designs as maintenance budgets need to be sustained as the entire bridge infrastructure continues to age.

As bridge structures continue to degrade, the disruptions for maintenance and repair will impair the bridge service that is required to sustain economic vitality, freedom of movement, defense, and emergency evacuation planning. For example, the I-526 bridges in Charleston, South Carolina had partial lane closures for weeks in 2018 due to

corrosion damage, resulting in major traffic disruptions for a large section of the municipality [2]. In part to address impacts on bridge service, accelerated bridge construction (ABC), as a construction philosophy and its associated technologies and innovations, have been introduced and implemented. ABC is wide in scope but its general view is to minimize the impacts of construction on the community. As such, designs incorporating ABC can be used on multiple facets of bridge construction. For example, the application of ultra-high performance concrete (UHPC) on the retrofit of bridge substructure elements have the benefit to strengthen existing bridge substructures (such as for the use with new superstructure construction) as well as ideally to provide a durable substructure.

UHPC has been touted as a durable construction material in terms of strength and service. The low water-to-cement content and use of pozzolanic materials in part creates a low permeability material that decreases ion transport (including chloride ions) and develops high electrical resistivity. Work by Farzad et al. 2018 [3], 2019 [4] showed that the use of UHPC in retrofit of corroded concrete can locally minimize corrosion macrocell coupling and provide benefit above conventional patch repairs that are still used. However, further testing on the extent of macrocell coupling for various repair geometries utilized UHPC is warranted. Development of an economical repair method to rehabilitate and protect bridge elements in severe environments as well as to increase the strength and performance of the bridge structure was of interest. Based on the promising characteristics of UHPC, using a thin layer of the UHPC on the damaged areas as a protective shell can be a solution for the problem being addressed. The application of a protective shell is suitable for retrofitting based on its low permeability, and its ability to increase the strength of the element, ease of cast, and reduce time and cost.

1.2. UHPC

Ultra high-performance concrete is comprised of cementitious materials and shredded fibers that allow for a high compressive strength greater than 126 MPa (18 ksi) and enhanced post-cracking tensile strength greater than 5MPa (0.7 ksi) [5-9]. In UHPC the

higher cement factor, in comparison to normal strength concrete (NSC) [10-11], provides an enhancement of the material density and strength [10, 12-18]. The low water-to-cement ratio (W/C) of UHPC (typically less than 0.25) and also the partial replacement of a portion of the un-hydrated cement with the pozzolanic components such as blast furnace slag, fly ash and silica fume allows for the high compressive strength and low permeability [19-23]. To improve the workability of the UHPC, superplasticizers are added to the mixture. Also, adding the silica fume can increase the workability of the mixture [13-14], [24-27]. The discontinuous pore structure of the low permeability UHPC reduces liquid ingress and significantly enhances the durability of the material to chemical degradation, including corrosion, compared to conventional concrete. Researchers have identified the beneficial permeability characteristic of UHPC. Schmidt.et al [28] and Techmann [29] identified lower porosity for UHPC in comparison to NSC . They reported total porosity (%) of UHPC to be 1.5 to 6 compared to 14 to 20 for normal concrete. Techman [29] further identified smaller capillary pore content for UHPC compared to NSC. The capillary pore (%) content was 1.5 for UHPC compared to 8 for NSC. The literature also showed that chloride ion transport is reduced in UHPC compared to NSC. Schmidt.et al reported very low chloride ion diffusivity (m^2/s) for UHPC in the order of 2×10^{-14} compared to values in the range of 10^{-12} to 10^{-9} for NSC. Graybeal [5] and Ahlborn [30] also compared UHPC to NSC by the standard test method for electrical induction of concrete ability to resist chloride ion penetration, ASTM C1202 [31]. For steam and air-cured specimens, Ahlborn [30] showed permeability less than 100 coulombs. Graybeal [5] investigated the chloride permeability based on different curing conditions. He reported 360 and 76 Coulombs permeability for untreated UHPC with the age of 28 and 56. Also, for steam, tempered steam, and delayed stem specimens with the age of 28 days, these numbers are reported as 18, 39, and 18, respectively.

Fibers in the form of steel, glass, and plastics are included in the concrete to increase its structural integrity, decreasing brittle behavior, reducing cracking tendency, and improving post cracking behavior [32]. The most common size of fibers is 13 mm (0.5 in.) in length and 0.20 mm (0.008 in.) in diameter with a recommended ratio of typical

2% by volume [5,16,26,33]. The mechanical property of cement-based material such as UHPC is significantly affected by the additions and distribution of the fibers. The distribution and orientation of the fibers can be caused by different factors, such as the workability of the mix, fiber content (volume) and method of casting, type and aspect ratio of the fiber, and how the fibers are introduced during mixing. Kang [34] found that fiber orientation is affected by the direction of the cast. Torrijos [35] showed fiber type, length, and casting methods significantly affected fiber orientation. Emdadi [36] showed that high fiber content decreases the UHPC workability, subsequently causes a non-uniform fiber distribution [32, 37-38].

Recent research identified the effect of fiber distribution and orientation on UHPC mechanical properties. Ferrara showed that non-uniform distribution of steel fibers in steel-fiber reinforced concrete adversely affected the mechanical behavior. Zhou [39] correlated the tensile ductility of engineered cementitious composite (ECC) to different steel fiber distribution. Kang [34] and Akacy [40] identified the effect of fiber orientation on mechanical performance. For example, Akacy [40] stated that the vertical orientation of fibers related to the bending direction enhances the flexural capacity. Similarly Kang [34] identified the effect of fiber orientation on the ultimate flexural strength, although there was a limited effect on the strength before the first cracking.

The fibers were also described to affect UHPC durability. Khayat et.al considered the effect of the fibers to facilitate the transport of charge by electronic transport through the conductive fibers. He reported by increasing steel fiber from 0 to 2% the UHPC resistance decreased by 40%. It was posited that fiber orientation could affect the transport of charge not only by electronic transport through the fibers but also by the preferred orientation of cement hydration grains and pores to facilitate ionic transport. The effect of fiber orientation on UHPC resistance caused by the flow of casting, fiber addition, and fiber type lacks at present.

1.3 Research Objectives

The objective of the research was to identify the extent to which construction of a UHPC shell to retrofit damaged concrete can mitigate corrosion. Electrochemical testing of reinforcing steel embedded in the core concrete of a damaged T-beam and within the UHPC shell was conducted to identify the extent to which macrocell coupling can occur in a large-scale test geometry including the effect of the extended cathodes coupled to a local corrosion anode. Furthermore, the research evaluated the effect of the fiber orientation on the electrical characteristic of UHPC by considering fiber presence and fiber type. Different test specimens with different fiber content, orientation, and different fiber conductivity were cast.

2. METHODOLOGY

2.1 Concrete Materials

Conventional normal concrete (NC) used in this study, provided by a local supplier, had a nominal compressive strength of 35 MPa (5 ksi). The mix design is shown in Table 1. The concrete slump was 102 mm (4 in).

Table 1. Concrete mix design.

Composition	UHPC	UHPC (Percentage by weight)	NC	NC (Percentage by weight)
Portland Cement (Kg/m3)	712	28.8	227	15.4
Coarse aggregate (Kg/m3)	-	-	747	41.6
Fine aggregate (Kg/m3)	1020	41.3	578	32.7
Silica Fume (Kg/m3)	231	9.4	-	-
Fly ash (Kg/m3)	-	-	57	3.2
Air-entraining agent (ml)	-	-	11	-
Ground Quartz (Kg/m3)	211	8.5	-	-
Accelerator (ml)	30	1.2	-	-
Total Premix (Kg/m3)	2204	88.0	1549	92.8
Superplasticizer (Kg/m3)	30.7	1.2	-	-
Steel Fiber(Kg/m3)	156	6.3	-	-
Water (Kg/m3)	109	4.4	129	7.2

The UHPC used in this research was the commercially available material, Ductal. The mixture composition of the UHPC is listed in Table 1. The fiber used in this research included steel and fiberglass fibers. The steel fiber was a straight steel fiber (length of 12.5 mm (0.5 inches) and radius if of 0.1 mm (0.008 inches)) with a density of 156 (kg/m^3). The steel fibers were braced coated, and the composition of its chemical elements is listed in Table 2. The glass fiber was an alkali-resistant commercial fiber (PH-950 x) with a length of 12.5 mm (0.5 inches). The density of the fiberglass was measured as 110 (kg/m^3).

Table 2 Steel fibers ingredients [5].

Elements	Composition (%)
Aluminum	≤0.03
Chromium	≤0.08
Sulfur	≤0.025
Phosphorus	≤0.025
Silicon	0.15-0.30
Carbon	0.69-0.76
Manganese	0.46-0.60

2.2 Large-Scale Test Specimen

As part of a larger study on the development of a durable repair method utilizing UHPC for damaged reinforced concrete elements, a large scale T-section deck was cast with simulated defects and was retrofitted. The T-section deck as the core of the section was cast with various modalities of degradation including concrete sections with chloride ion contamination. The concrete core surface was roughened by sandblasting (in part to simulate the removal of delaminated concrete) and a UHPC repair shell was cast around the core.

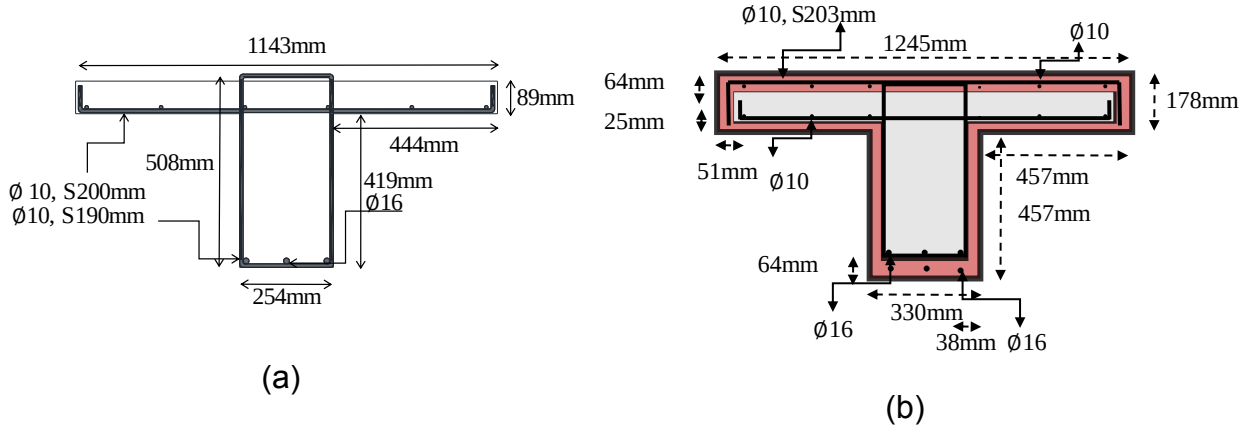

Figure 1. T-section deck section detail: (a) Damaged section; (b) Retrofitted section.

Figure 1 shows the section of the deck representing a damaged section and the retrofitted section. The dimensions of the damaged deck were 1143 x 89 mm for the

flange and 254 x 419 mm for the web. The damaged section has three ø16 longitudinal reinforcements in the web with a cover of 10 mm from the bottom of the web and six ø10 longitudinal reinforcements in the flange with a cover of 71 mm from the top of the flange. The flange and web also have transversal ø10 reinforcement at 200-mm and 190-mm spacing; respectively. Figure 2 shows the sequence of casting and demolding the core section of the T-beam. Figure 3 shows the sequence of concrete core surface preparation. The test specimen was delivered to a local sandblasting shop and the surface of the concrete was roughened by sandblasting to facilitate bond with the UHPC overlay to be subsequently cast. In addition, mechanical connectors (made of rebar ø10 with a length of 57 mm) were secured to the surface of the concrete core section by securing the steel dowels 13 mm deep in drilled holes with an anchoring adhesive.

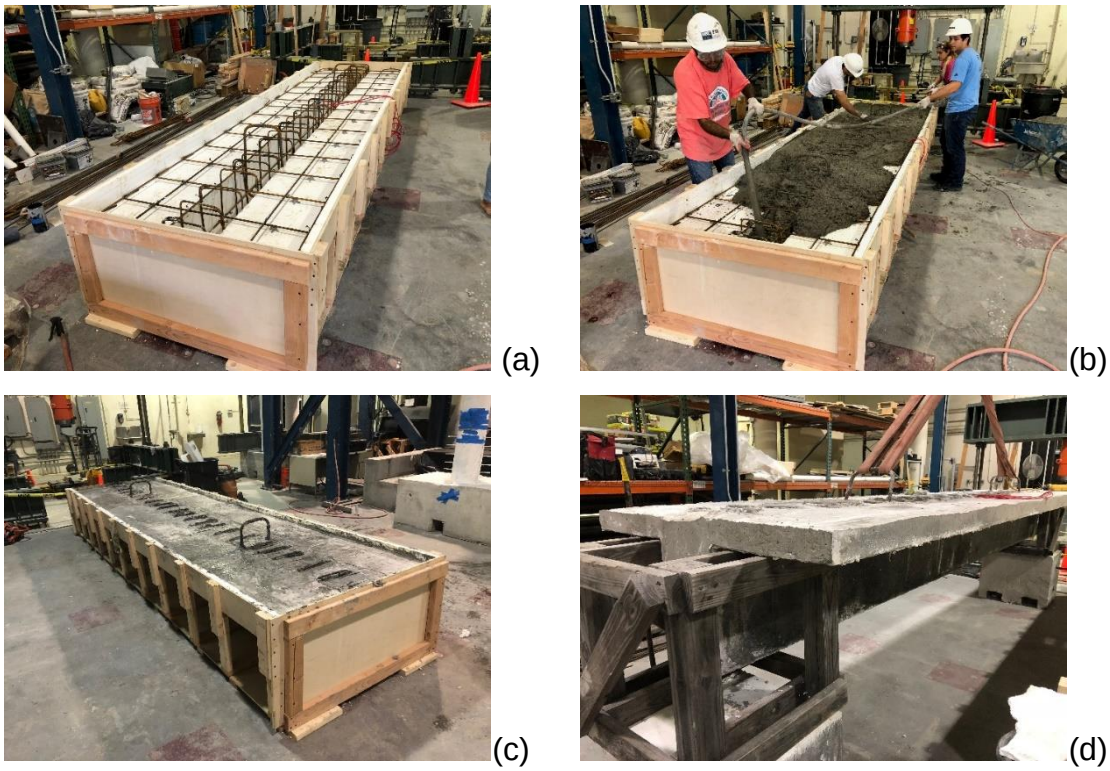

Figure 2. T-Beam test specimen: (a) Formwork of the initial damaged section; (b) Casting conventional concrete in the formwork; (c) Test specimen after casting; (d) Test specimen after demolding.


(a)
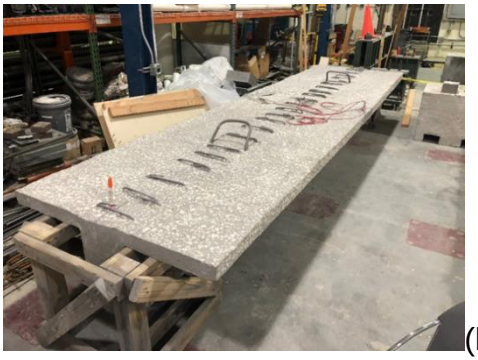
(b)

(c)

(d)

Figure 3. Surface preparation of T-beam specimen core: (a) Sandblasting in progress; (b) Roughened surface after sandblasting; (c) The mechanical connectors on the flange; (d) The mechanical connectors on the web.

The core section of the T-beam specimen was placed into a mold with dimension as shown in Figure 1b. The mold was made of a transparent acrylic material so that the flow of the UHPC repair material could be visually monitored during casting (Figure 4). The spacing between the concrete core and the mold around the side and bottom perimeter was 76 mm. Three ø16 reinforcements were added at the bottom of the formwork web and 6 ø10 longitudinal reinforcements were combined with ø10 transversal reinforcement at 203 mm spacing were added to the top of the flange (to be embedded in the repair UHPC shell as part of extended testing of mechanical beam performance). All additional reinforcing steel had a cover of 38 mm. As will be described later, the steel in the concrete core as well as the additional reinforcing steel embedded in the UHPC shell were instrumented for electrochemical testing.

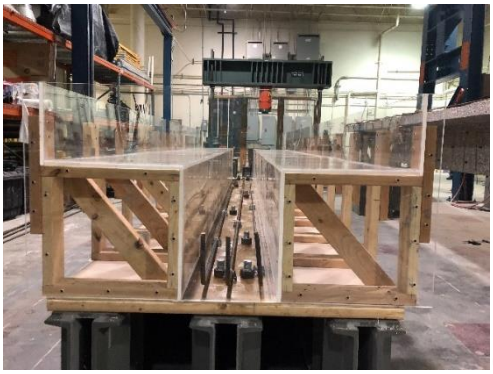 (a) 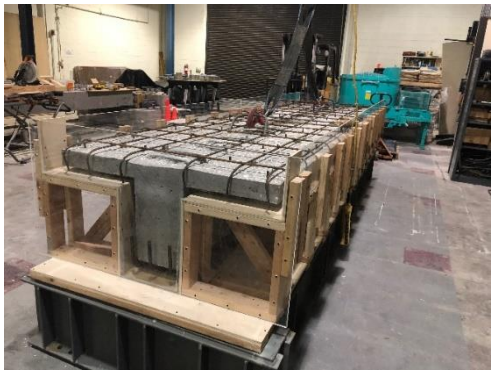 (b)

Figure 4. Construction of formwork for the UHPC repair: (a) The acryllic formwork; (b) Placement of addition reinforcing steel in the beam flange.

2.3 T-Beam Electrochemical Testing

The corrosion durability of the UHPC shell was investigated by periodically measuring the open-circuit potential of the steel embedded in the UHPC shell as well as the macrocell corrosion current between embedded steel in a portion of the T-beam containing chloride contamination and the extended array of cathodes in the beam core and the UHPC repair.

As described in the previous section, after the concrete core section was initially cast and cured, additional reinforcing steel was placed to be embedded in the UHPC encapsulation shell. However, prior to the casting of the UHPC, a portion of the concrete core flange at one end of the T-beam was overlaid with NC concrete in two segments (dimension of 571 x 508 x 64 mm) as shown in Figure 5. One of the NC concrete segments was contaminated with sodium chloride (8% of cement mass) so that a region of the test specimen would represent a portion of a beam with vestigial chloride content after the UHPC repair. The high chloride content was made to ensure development of corrosion anodic regions in the test specimen. The reinforcing steel in this segment would develop a local anode to be coupled with the extended cathodes from the steel in the NC concrete core as well as in the UHPC shell. All of the added transverse and longitudinal reinforcements were cast electrically isolated from the steel in the concrete core and each other. Intersecting rebar were separated by rubber pads. This isolation would ideally provide an opportunity to measure the macrocell corrosion current that would develop between the steel in the chloride region with the extended

cathodes in either the core or in the UHPC shell via external electrical switches. The reinforcing steel was instrumented by attaching copper wires to stainless mechanical studs drilled into each rebar. After casting, the individual rebar were interconnected using electrical switches and was usually kept on the on position except for short term disconnects for the macrocell current measurements.

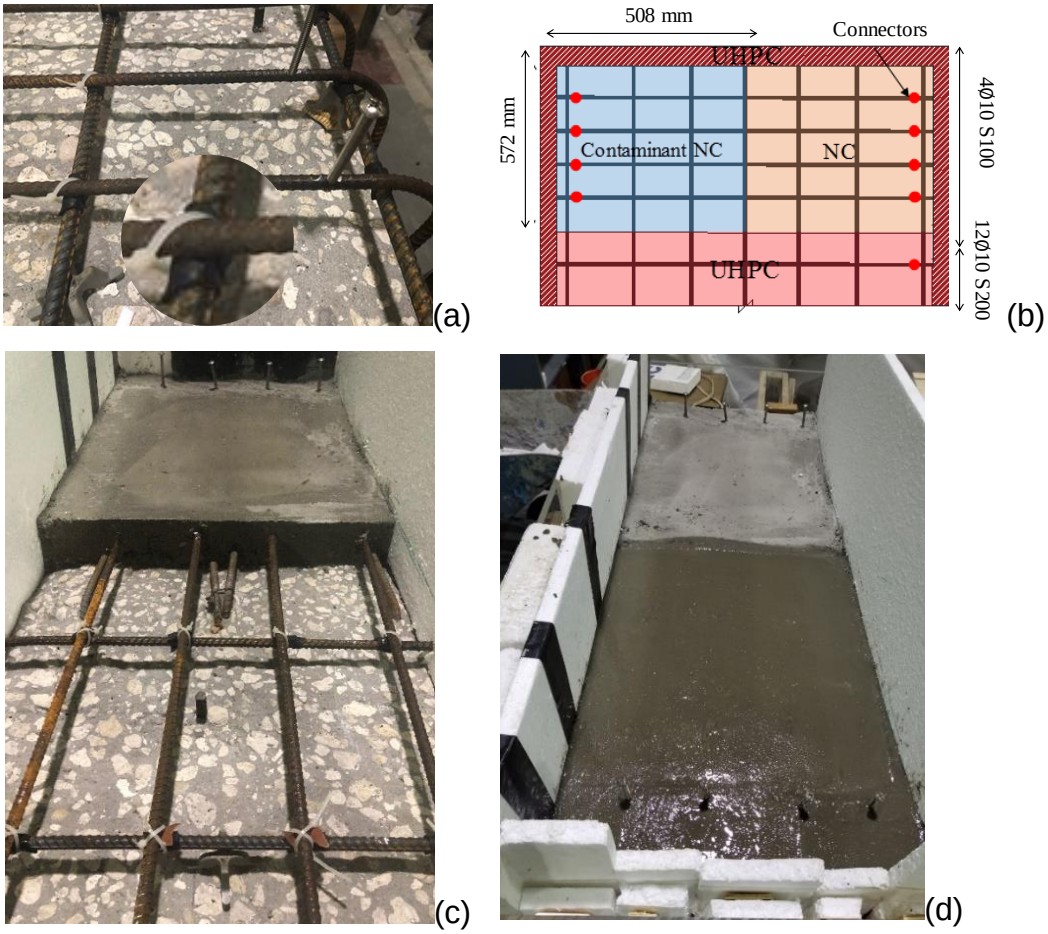

Figure 5. Local anodes in flange NC concrete segment of retrofitted T-beam specimen. (a) Electrical isolation of intersecting rebar and electrical connectors. (b) Schematic of NC section. (c and d) Cast NC sections with and without chloride contamination.

Corrosion half–cell potential measurements of the electrically interconnected steel rebar (via the electrical switches) were used based on the ASTM-C876 standard to measure the corrosion activity of the steel reinforcement. A copper/copper-sulfate electrode (CSE) was used as the reference electrode. For the test, an electrical connection was

made between the reference electrode and the contact points of the reinforcing steel via a high impedance voltmeter. The half-cell potentials were recorded at multiple locations of the T-beam deck in a grid to verify the corrosion activity The grid was made such that each reading point coincided with the location of the reinforcing steel (Figure 6). If sufficient readings are taken on a grid pattern (half-cell corrosion mapping), a contour map can be prepared, which can show the different locations of the deck with the highest probability of corrosion activity.

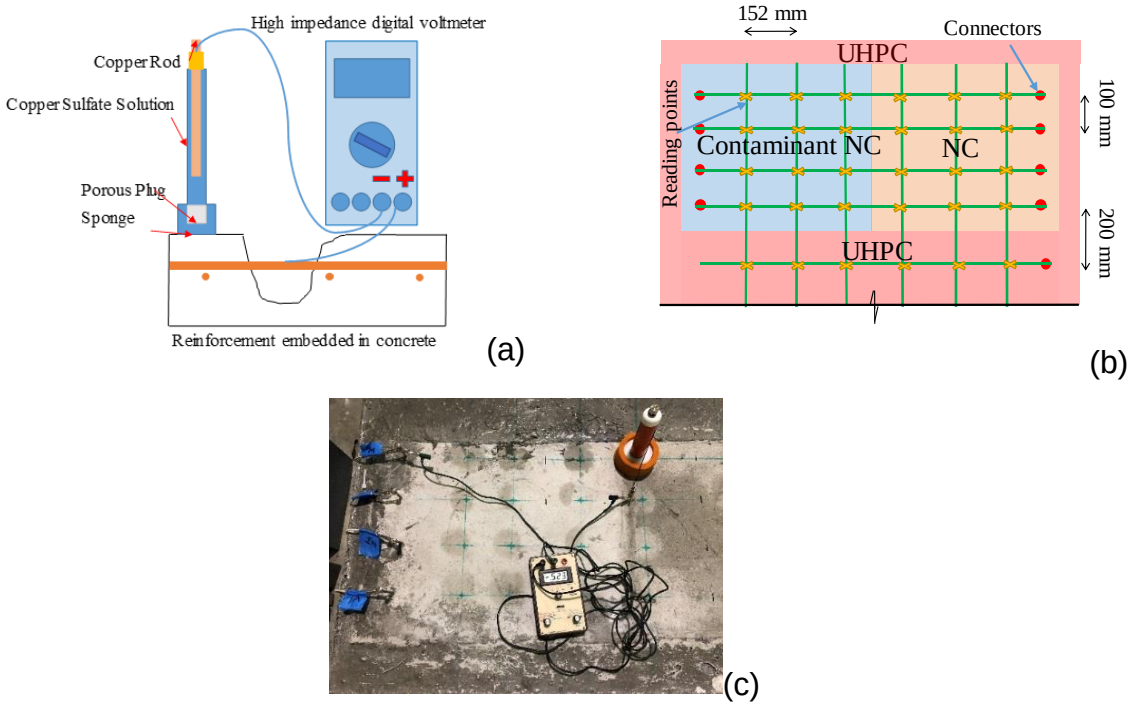

Figure 6. Half-cell Potential Measurements. (a) Schematic of connections; (b) Measurement grid pattern; (c) Photograph of measurement on beam top flange.

To investigate the extent of macrocell coupling of steel in the perimeter of the beam from the UHPC repair, the macrocell current between the corroded rebar in the normal concrete section as the anode and encapsulated rebar in UHPC section, as well as the rebar embedded in the core (damaged normal concrete section), was measured. The rebar in the anode and cathode sections, initially electrically isolated, were connected by external wires terminating at an electrical switch box (Figure 7) The electrical switch box allowed for the connection of the corroding rebar in the chloride-contaminated NC

section and the transverse rebar in the UHPC flange repair as well as separately to the NC core section. The bars in the UHPC repair could individually connected or disconnected to vary the size of the extended cathode in the UHPC repair material. This macrocell current measurement ideally would identify the extent of adverse macrocell coupling based on the different cathode to anode ratio.

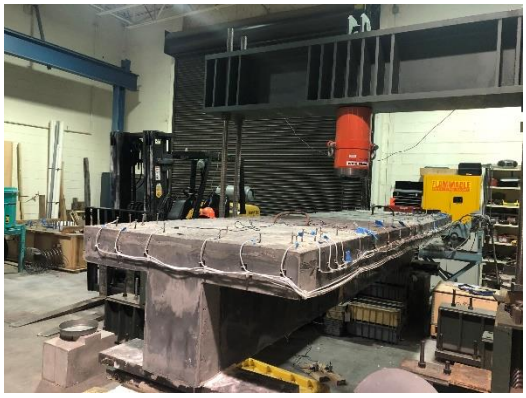

(a)

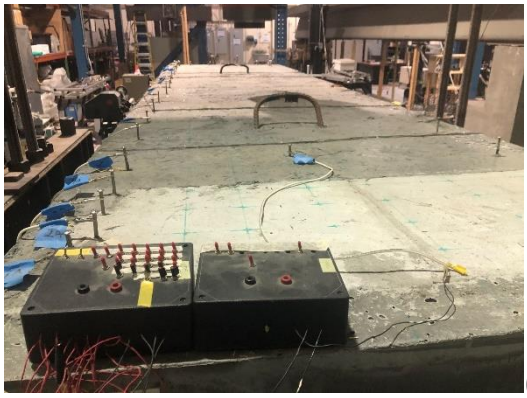

(b)

Figure 7. Macrocell current measurement:(a) External wires connecting the rebar .(b) The electrical switch box.

2.4. Electrical Characteristics of Fibers in UHPC

Small scale test specimens were cast to investigate the effect of the chopped fibers on the electrical behavior of the UHPC. A pan mixer with a 20-liter capacity and stirring shaft speed of 195 (r/min) was used (Figure.8). The UHPC premix was blended for 3 to 5 min. Then, a part of the superplasticizer (SP) volume was gradually added to the premix with the mix water and mixed for 15 min. The remaining portion of the superplasticizer was added and mixed for another 2 to 3 min allowing the mix to become fluid. In this step, the different types and dosages of fibers were gradually added to the mixture to allow for uniform blending. After adding the fibers, the concrete was mixed for an additional 6 min prior to the casting.

The specimens were cast as small beams with the dimension of square section 76 mm x 76 mm (3 in. x 3 in.) and length of 608 mm (24 in.). To facilitate the parallel alignment of the fibers along the length of the beam, the formwork was held at 45 degrees during

casting. The vertical deviation allowed the UHPC to smoothly flow parallel to the length of the beam and ideally allow the fibers to orient itself with the streamline. The rheology of the fresh UHPC was evaluated using ASTM C1437 (Figure 8). The results of the flowability test are listed in Table 3. The glass fibers apparently absorbed water and resulted a smaller static flow. Control test specimens with no fiber content were likewise cast.

The electrical resistivity of concrete relates to its capability to resist the movement of ions such as in an electrical field. The electrical resistivity is a material characteristic relating to the concrete porosity, moisture content, and concrete temperature. The microstructural properties of concrete including the pore size and tortuosity also can affect the transport of charged species. The two-point and four-point resistance measurements can be used to assess the concrete electrical resistivity. The two-point technique is used for concrete bulk resistivity measurement, and a four-point technique is used for surface electrical resistivity.

Electrical testing of the concrete specimens consisted of two-point resistance measurements utilizing a Nilson soil resistance meter and electrochemical impedance spectroscopy using a Gamry Ref600. The resistance measurements were made in a series of tests utilizing combinations of cut concrete segments. Initially, each beam was cut into 76 mm (3-inch) segments and each cut surface was ground to provide a uniform surface roughness. Each segment was environmentally conditioned in 100% RH curing chambers. For testing, the segments were arranged by holding consecutive segments in series, each separated by a wet sponge, with a c-clamp. Two steel plates cut to the dimensions of the beam cross-section were used as the end electrodes. Wet sponges were used to provide better surface contact of the electrodes to the concrete surface.

The EIS measurements were made with 0V DC bias and a 10 mV ac perturbation voltage with a frequency range of 1MHz to 1 Hz (10 points measured per decade).

Table 3 The rheological properties of the test mixes.

Specimen	Static Flow	Dynamic Flow
Steel Fiber 4%	198 mm (7.8 in)	220 mm (8.7 in)
Steel Fiber 2%	218 mm (8.6 in)	241mm(9.5 in)
Glass Fiber 4%	90 mm	-
Glass Fiber 2%	100 mm	-

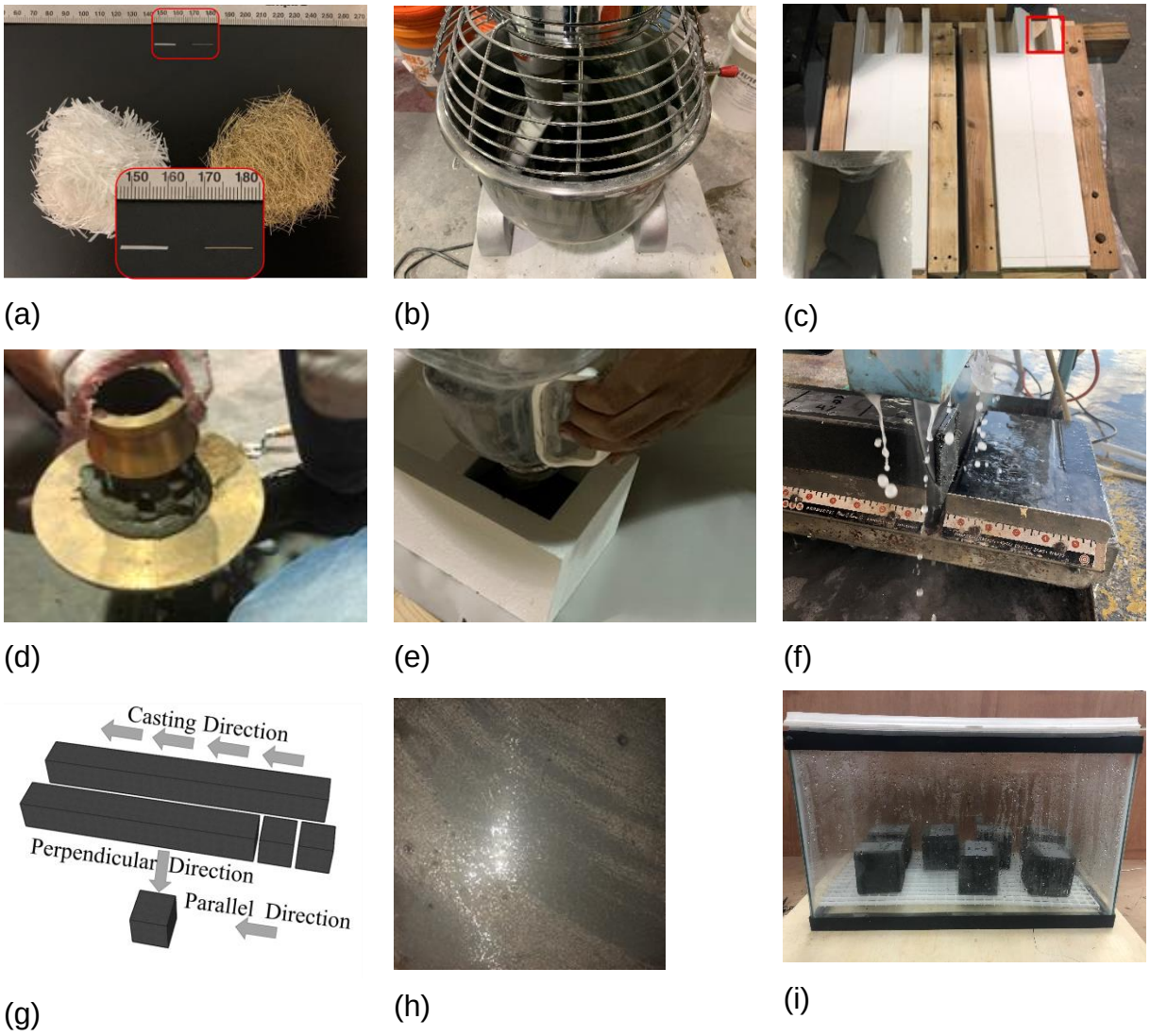

(a) (b) (c)

(d) (e) (f)

(g) (h) (i)

Figure 8. Test specimens preparations (a) Fibers, (b) Mixing process (c) Casting Process, (d) Flowability, (e) Reference specimen, (f) Cutting process, (g) Cast and cut directions, (h) UHPC surface after grinding, (i) Curing condition.

3. RESULTS AND DISCUSSION

3.1 T-Beam Electrochemical Testing

The results of the half-cell potential mapping at day 25, 56 and 100 are shown in Figure 9. Based on ASTM C876, if the reinforcement potential is less than -0.35 V_{CSE}, the probability of having corrosion activity is close to 95 percent. When the potential is between -0.20 and -0.35 V_{CSE} the corrosion is uncertain. Passive conditions typically develop at potentials more noble than -0.20 V_{CSE}. As shown in Figure 9, the steel embedded in the chloride contaminated concrete shown in the regions between 0 and 30 cm labeled anode 1-4 developed highly electronegative potentials indicative of the expected corrosion activity there. The electrical potentials of the rebar embedded in the chloride-free NC (45-75 cm) developed moderate potentials in the range of -0.2 to -0.4 V_{CSE} even though passive corrosion conditions was expected there. All of the rebar embedded in the UHPC (Cathode 1-16) all developed passive potentials (except for a small portion at the edge of the deck). The moderate potentials developed in the chloride-free NC concrete was related to the coupling of the actively corroding steel in the chloride-contaminated region and shows that there can be significant polarization of the adjacent steel embedded in the rather poor quality concrete (lower resistivity). This enhanced cathodic polarization of the adjacent steel (throughout the entire length of the NC region, over 45 cm) in the chloride-free NC concrete would enhance the rate of cathodic oxygen reduction there and support elevated macrocell corrosion of the steel in the chloride-contaminated region. Conversely, this polarization did not occur for any of the steel rebar embedded in the UHPC (including those directly adjacent to the NC region, 20 cm away and further). This observation highlights the effect of the high quality UHPC to minimize the extent of macrocell coupling of the anodes to the extended cathodes in the steel embedded in the shell repair.

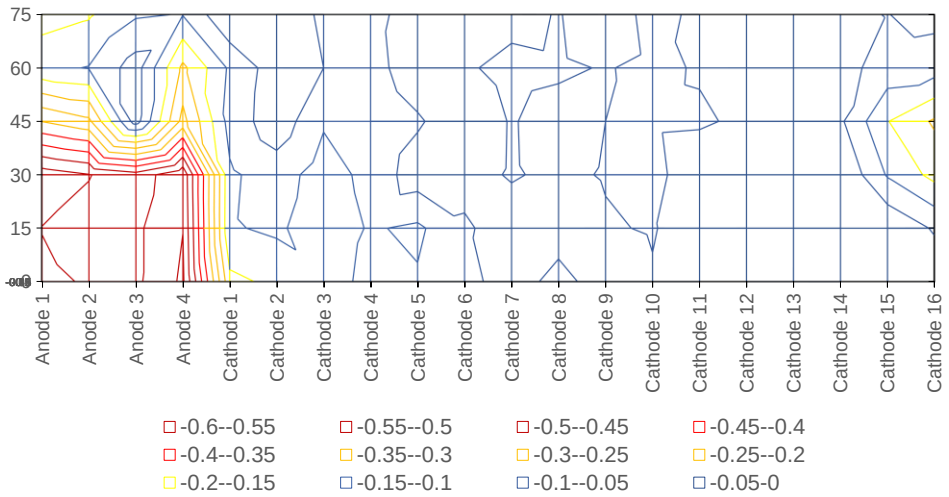

a)

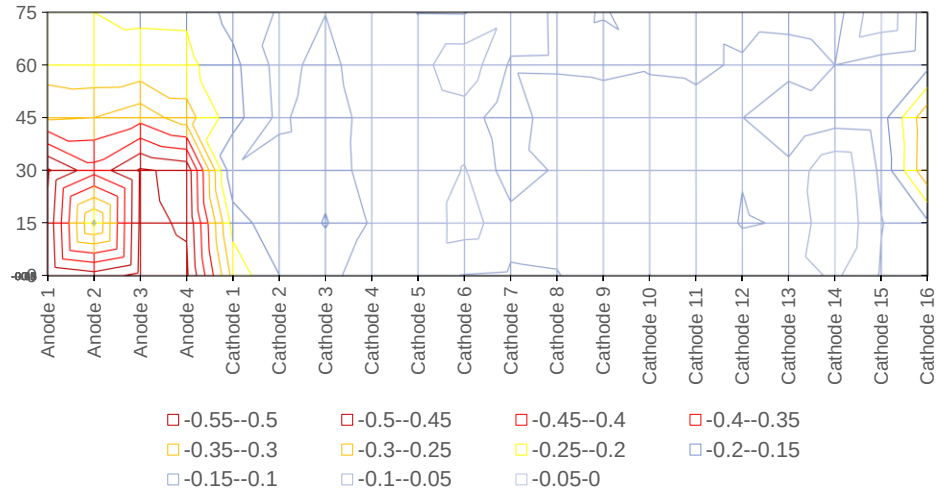

b)

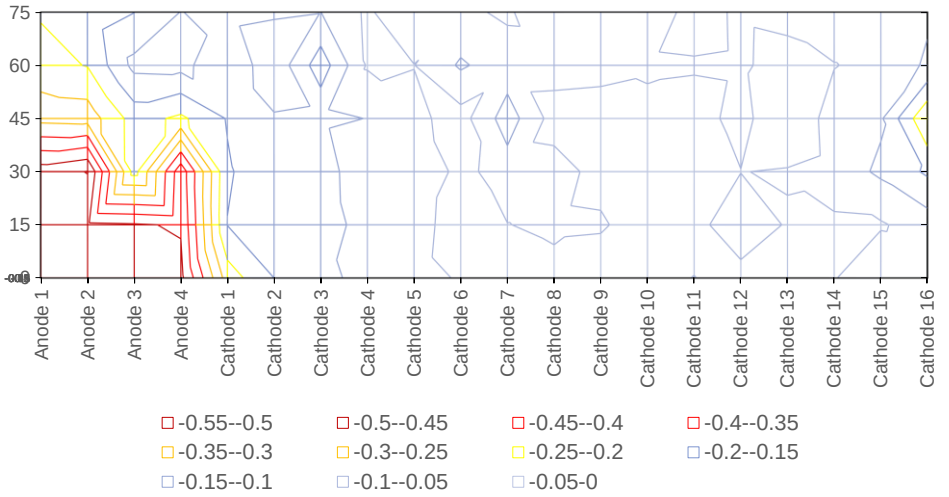

c)

Figure 9. Half-cell potential mapping of deck surface. Contours in V_{CSE} a) Day 25. b) Day 56. c) Day 100.

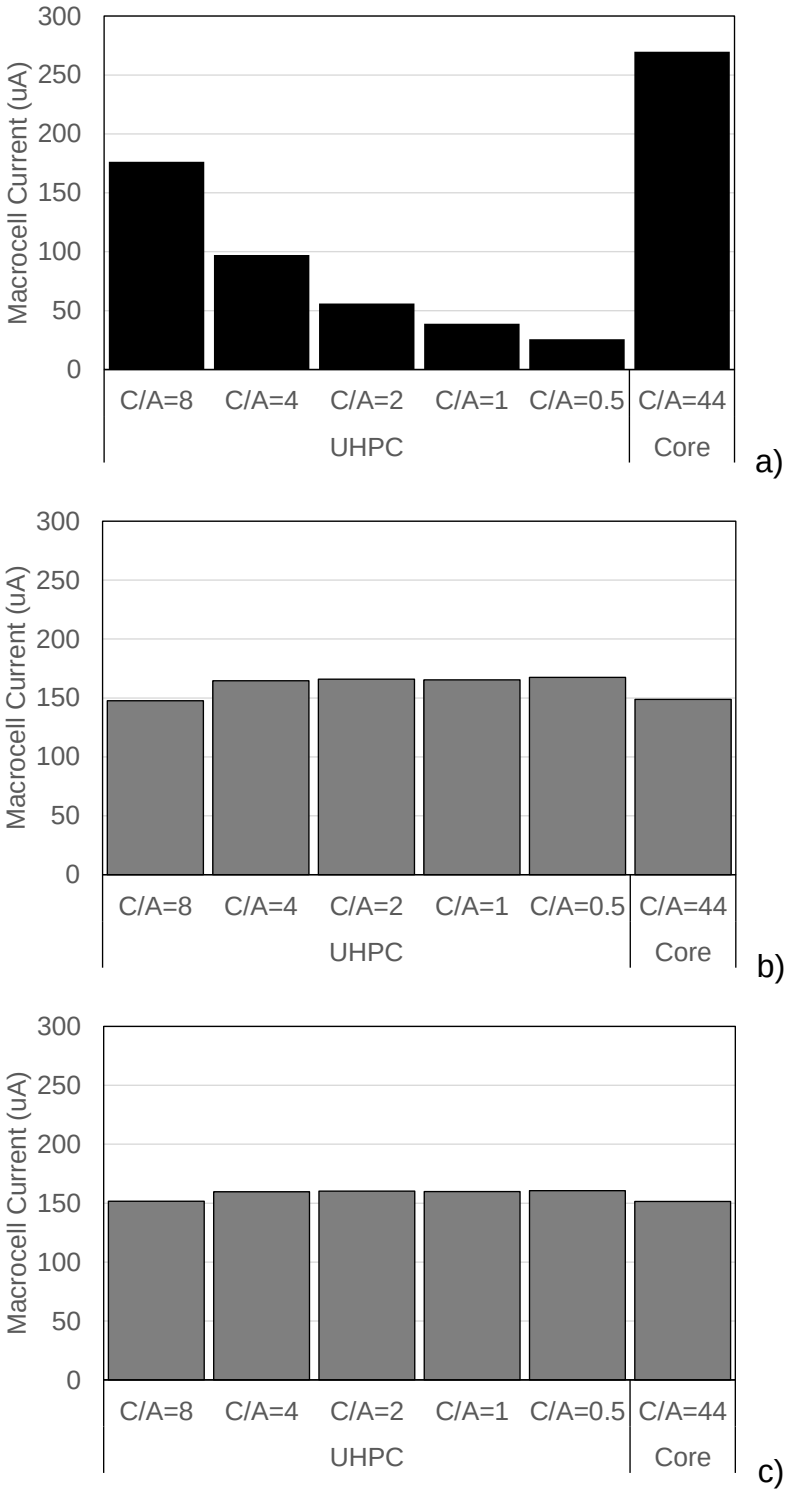

Figure 10. Macrocell current between anode and UHPC or core concrete cathodes. C/A: Cathode-to-Anode Ratio.
a) Day 36. b) Day 56. c) Day 100

The results of the macro-cell current measurements between the anodes in the chloride-contaminated NC concrete and the steel in the UHPC repair as well as for the steel in concrete core substrate at days 36, 56, and 100 are shown in Figure 10. At day 36, there was a clear linear relationship between the macrocell current and the cathode-to-anode ratio for the cathodes in the UHPC repair. The larger extended cathode in the UHPC allowed for larger macrocell currents to develop. It is noted that the macrocell current was much larger when the cathode was the steel embedded in the concrete core substrate. Even though the embedded steel there would be encapsulated with the UHPC that could minimize oxygen transport, there would be sufficient oxygen in the substrate concrete pore water to support the cathodic oxygen reduction reaction.

Subsequent macrocell current measurements at day 56 and 100 showed a change in macrocell behavior. For all cases, a similar macrocell current was measured regardless of the cathode-to-anode ratio. The macrocell current was likewise similar when coupled with the steel in the core substrate concrete. The similar current for all test conditions may reflect a base current between the anodes and cathodes within the NC region and that the UHPC and that the UHPC restricts the level of oxygen reduction in the UHPC repair section. However, it cannot be ruled out that instrumentation of the rebar may have been compromised during relocation of the test specimen after the initial measurement.

3.2 Effect of Fibers on UHPC Electrical Resistance

The use of UHPC in the retrofit of reinforced concrete elements was posited to provide extended corrosion durability not only by the low permeability characteristics of the material but also by reducing the extent of macrocell coupling of cathodes embedded in the UHPC. The low permeability of the cementitious component of the UHPC would allow for high electrical resistance; however, the presence and orientation of the fibers were posited to have an effect on the overall concrete electrical resistance. Different fiber contents, orientations, and different fiber conductivity were assessed. Digital Image processing (DIP) was implemented to assess the fiber orientation, and the electrical

property of each sample was assessed by two-point electrical resistance (ER) measurements and Electrochemical Impedance Spectroscopy (EIS).

3.2.1 Digital Image Processing (DIP)

DIP was implemented to provide quantitative characterization of the fiber distribution along the length of the test specimen. From each cast beam, three cut sections (from the the middle and 76 mm (3 inches) from each end of the beam) were evaluated (Figure 11). The cut specimens were heated in the oven for 30 min with the average temperature of 150 ºC (302 ºF) and allowed to cool in the ambient laboratory conditions at a temperature of 23 ± 2 ºC (74 ± 3 ºF) for 5 minutes to create differential temperature between the fibers and concrete. A FLIR thermal infrared camera was used to capture thermal images of the concrete section surface. To mitigate the effect of differential cooling of the edges of the concrete, the prepared images were cropped from the size of 76 mm x 76 mm (3 in x 3 in) to the size of 38 mm x 38 mm (1.5 in x 1.5 in) as shown in Figure 11d. The images were digitally processed in a MATLAB program as described next. First, the contrast filter was applied to the images to better differentiate the fibers from the concrete [41]. The enhanced images were subdivided into 16 equal-sized images. The individual images were changed from RGB format to the gray-scale images with a pixel intensity between 0 to 225. The threshold filter was then applied to change the image into black-and-white format with the pixel intensity between 0 to 1 [42]. The total surface area of the fibers and the concrete could be estimated by the number of white and black pixels, respectively. The population density (ρ) of the fibers was measured Equation 1.

$$Fiber\ density(\rho) = \frac{Area\ of\ fibers}{Total\ Area\ of\ the\ section} \qquad (1)$$

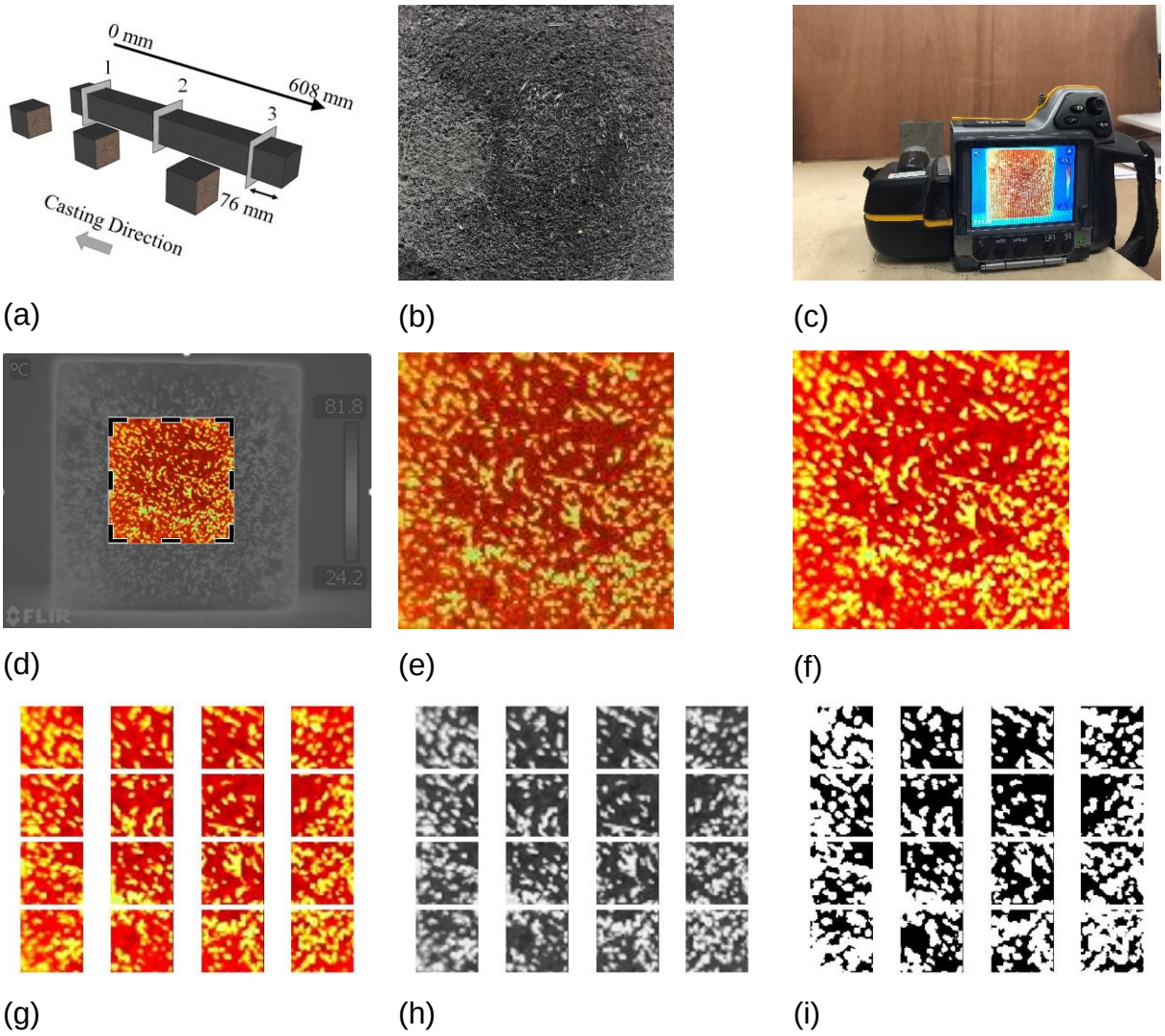

Figure 11. DIP method (a) Cross sections used for analysis, (b) The specimen with 4% fiberglass, (c) The image from infrared camera, (d) The cropped image section, (e) The RGB image transferred to the MATLAB, (f) The enhanced image, (g) Segmentation of enhanced image, (h) Gray-scale image, (i) The blacked and white image.

The fiber orientation was characterized by the angle made between the normal direction of the cut surface and the fiber axis ($\boldsymbol{\alpha}$) as illustrated in Figure 12 with using Equation 2. A fiber orientation coefficient ($\boldsymbol{\gamma}$) was defined as in Equation 3 where $\boldsymbol{\gamma}$ can change between 0 and 1 while the fibers are aligned parallel or align perpendicular to the cross-section [34, 43].

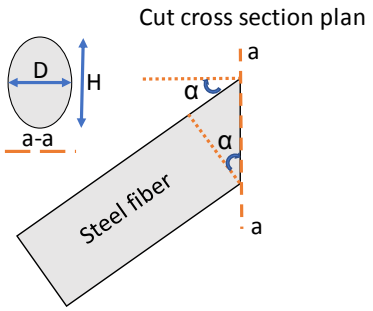

Figure 12 Fiber inclined angle illustration

$$\alpha = arccos(\frac{D}{H}) \quad (2)$$

$$\gamma = \int_{\alpha_{min}}^{\alpha_{max}} p_\alpha \, cos^2\alpha d\alpha \quad (3)$$

where p_α shows the probability distribution of fiber for fibers with angle α [44].

Figure 13 shows the cross-section thermal image of the UHPC specimens cast with 2 and 4% steel fiber. It was evident that the steel fiber orientation was generally aligned parallel to the cast direction as shown by the minimal transverse cross-section of each fiber. After the digital image processing to delineate the fiber periphery, the fiber population density, ρ, and orientation, γ values for each cut concrete section face was calculated using Equation 1 and 3, respectively. Table 4 lists the average ρ and γ for each section. As expected, the calculated fiber density ρ on each section profile for the UHPC mix with 4% fiber was higher than the UHPC with 2% fiber. The average ρ values for the profiles at specimen mid-length were 0.45 and 0.35 for the 4% and 2% UHPC mix, respectively. Furthermore, the average fiber orientation coefficient γ was greater than 0.7 for all profiles, consistent with the visual observation of the parallel alignment of the fibers for both the 4% and 2% UHPC mixes.

As presented earlier in Table 3, it was evident that the fiber content had an effect on the UHPC rheology. The flow test results confirmed that the UHPC pre-mix and the fiber components were well mixed for all test specimens. The workability of the UHPC with the higher fiber content was lower than the UHPC with the lower fiber content. This was

due to the higher overall friction between the fiber and the cement matrix during the casting with the larger fiber population [45-46]. Research in the literature attests to this effect of the fiber content and geometry on the workability of fiber-reinforced concrete. This effect by the fiber content was manifested by the trends of the average calculated ρ values along the specimen length. For example, the 4% UHPC mix (with the lower workability) generally had uniform fiber distribution along the entire specimen length (ρ ~0.35-0.45); whereas, the 2% UHPC mix (with higher workability) showed a major drop in ρ from 0.3-0.35 (at 12 and 21 inches from the casting point) down to <0.1 (at 3 inches from the casting point). Furthermore, the observed fiber segregation for the 2%-fiber UHPC mix allowed for the aggregation of the fibers downstream, consistent with the lower but similar calculated ρ values (i.e. ρ~0.3-0.45) relative to the 4%-fiber UHPC mix at sections 1 and 2. The results showed an indication that the UHPC mix with higher workability allows for better-aligned fibers in the direction of casting. Specimens with 2% fiber showed γ values (0.8-0.91) generally higher than the specimens with 4% fiber (0.74-0.81). For the specimens with the glass fiber (in part relating to the light weight of the material and more cohesive bond), the fibers were oriented randomly which resulted in a more uniform distribution of the fibers.

Table 4 Fiber distribution and orientation along the length.[1]

Specimen	Section 1		Section 2		Section 3	
	ρ	γ	ρ	γ	ρ	γ
Steel Fiber 4%	0.4	0.78	0.45	0.81	0. 35	0.74
Steel Fiber 2%	0.3	0.8	0.35	0.84	0.06	0.91
Glass Fiber 4%[2]	-	-	-	-	-	-
Glass Fiber 2%[2]	-	-	-	-	-	-

1. Average values calculated from measured values for each profile subdivision. 2. Glass fibers were not well distributed. ρ and γ were not calculated.

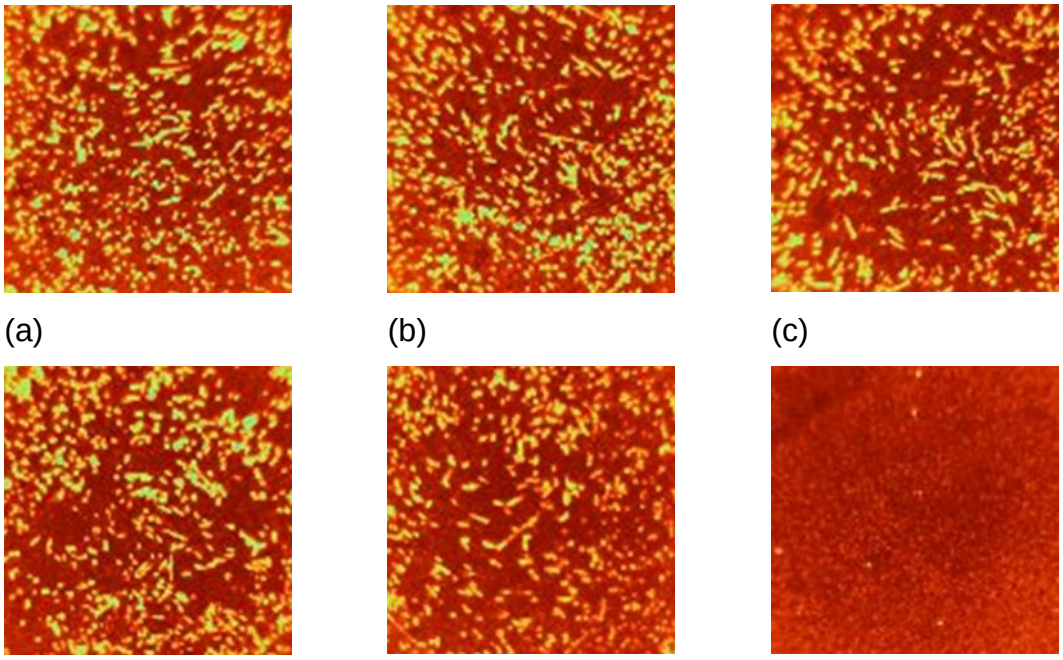

(a) (b) (c)

(d) (e) (f)

Figure 13. Fiber distribution and orientation (a) Steel fiber 4% section 3(top), (b) Steel fiber 4% section 2 (middle), (c) Steel fiber 4% section 1(bottom), (d) Steel fiber 2% section 3 (top), (e) Steel fiber 2% section 2(middle), (f) Steel fiber 2% section 1(bottom).

3.2.2 Electrical Resistance

The two-point resistance tests utilizing a soil resistance meter were made on the concrete segments after 28 and 56 days of exposure in the 100% RH chamber. All concrete specimens were surfaced dried with a towel prior to testing. Two parallel stainless-steel plate electrodes were placed on the each end of the concrete test specimen with moist sponges and held in close contact with a c-clamp (Figure 14). Excess surface wetting of the specimen was avoided to prevent possible preferential charges through the outer surface of the concrete. The measurements were made in a sequence for each material where each cut concrete section was sequentially added in series and held in close contact via the wet sponges and the clamp. The concrete sections were added such that the fibers were either aligned along the longitudinal length of the specimen (parallel to the applied current path) or each rotated 90 degrees so that the fibers were aligned perpendicular to the length of the specimen (orthogonal to the applied current path). The total resistance was corrected afterward by deducting the electrical resistance of the added sponges.

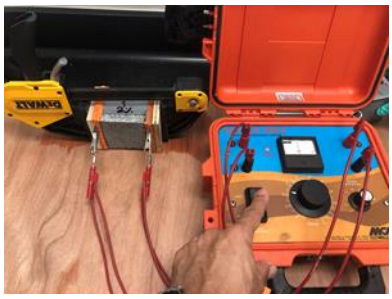

(a)

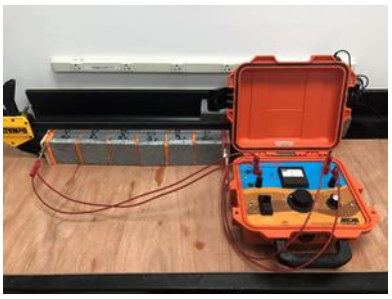

(b)

Figure 14. Resistance Measure of the Samples Segmental (a) Section, (b) Sections Connected by Sponge.

The concrete bulk resistivity was calculated by Equation 4

$$r = R\frac{A}{L} \qquad (4)$$

where r is the resistivity of the concrete (Ω.m), R is the resistance (Ω), A is the cross-sectional area of the samples 5800 mm^2, and L is the total length of specimen 76 mm to 610 mm.

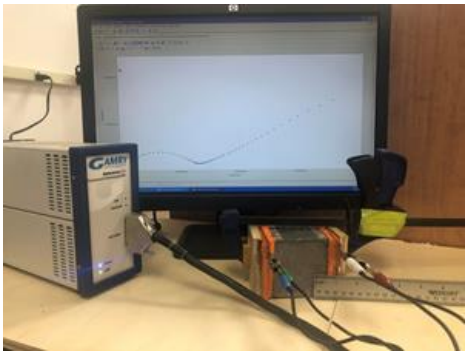

Figure 15 EIS measurement of each sectional sample.

The analysis of concrete by EIS is based on the electrical characteristics of its components. The only conducting path was through the pore solution in the macro, capillary, and gel pores. As a first approach, the charge transport through the concrete can be considered to be uniform, and an equivalent circuit, as shown in Figure 16 can be considered representative of the test system where CPE_c and R_{po} represent the capacitive and resistive behavior of the concrete matrix, and CPE_{dl} and R_{ct} are the

double-layer capacitance and charge transfer resistance at the electrolyte-steel electrode interface at the two steel electrodes. If the impedance associated with the steel interface at both electrodes are the same, the impedance spectrum in the Nyquist representation would give two separate impedance loops such as depicted in Figure 16 and the total impedance can be represented by Equation 5.

$$Z = \frac{1}{Y_{oc}(j\omega)^{nc} + \frac{1}{R_{po}}} + \frac{1}{Y_{odl}(j\omega)^{ndl} + \frac{1}{R_{ct}}} \qquad (5)$$

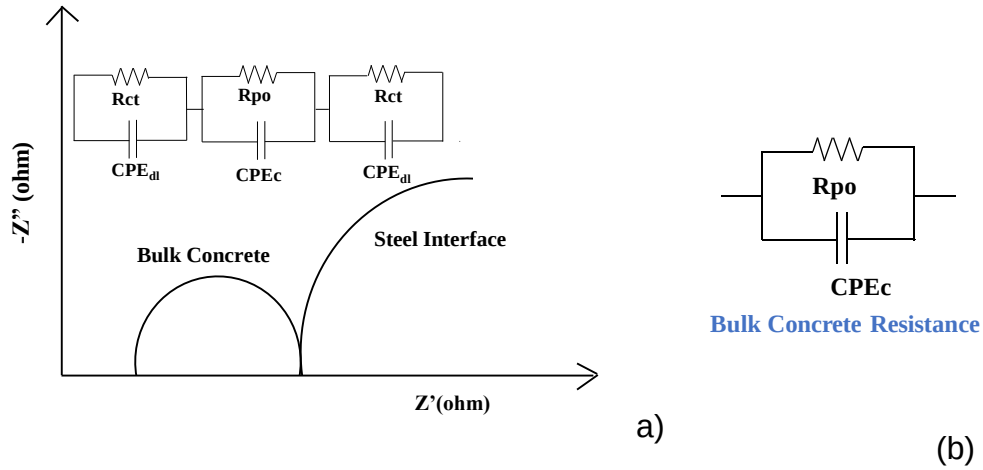

Figure 16. Schematic of impedance spectrum with (a) electrical equivalent circuit of the system and (b) equivalent circuit of the concrete.

In the Nyquist plot, the R_{ct} and CPE_{dl} represent the impedance associated with the low-frequency response of steel electrode interface and is not considered relevant to the work here. Consequently, the high-frequency impedance loop can be described by the equivalent circuit in Figure 16b.

Figure 17 shows the bulk resistance of the UHPC samples with 2% and 4% steel and fiberglass fibers along different lengths of concrete sections connected in series with the fiber orientation in parallel or orthogonal to the electrical current path with hydration time. As expected, the electrical resistance for all materials was lower with the shorter specimen lengths due to the shorter path for charge to travel and lower at the earlier hydration time (and shorter exposure in the 100%RH chamber) due to the shorter time

for the clinker to hydrate and the shorter time for moisture penetration from the conditioning environment. Specimens with 2% steel fiber showed slightly higher resistance than samples with steel 4% fiber. This can be due to the greater resistance to ionic charge motion with the greater presence of the high quality cementitious materials in the former. However, it was posited that the lower electrical resistance with the higher steel fiber content allowed for contributing electrical charge through the metal in the presence of the electric field impressed during the measurement. Indeed, in contrast, the poorly conductive fiberglass showed somewhat larger resistance with the higher fiber content.

The experiments were repeated with the concrete sections arranged so that the fibers were aligned orthogonal to the electrical current path. Figure 18 shows the results for steel and fiberglass fibers. It was evident that the orientation of the steel fibers have significant influence on the overall bulk UHPC resistance. In all cases, specimens with the steel fiber aligned orthogonal to the current path resulted in larger electrical resistance in comparison to when the steel fibers were aligned parallel with the current path. This effect was not observed for the specimens cast with fiberglass. Also, the overall electrical resistance was lower for the specimens cast with steel fibers than the less conductive fiberglass fibers.

Figure 19 presents a summary of results for the various test conditions. The UHPC without fibers showed significantly larger (up to an order of magnitude) resistivity. UHPC with steel fibers showed the lowest resistivity, and UHPC with fiberglass showed somewhat higher resistivity. Only specimens with steel fibers show a difference in resistivity with the fiber orientation.

The results show that the presence of fibers have an effect to reduce the overall electrical resistivity likely in part related to partial volume replacement of high quality cement and possibly oriented pathways in the cement microstructure along the fiber interface that can facilitate ionic movement. These ionic paths in the cement microstructure would be expected to be better manifested for the specimens with the

fibers cast in parallel with the current path, although no significant enhancement was observed for the cases with the fiberglass. Indeed, the results would suggest rather that the parallel orientation of conductive fibers with the current path at high enough concentrations can create a system where electronic charge through the conductive fiber can be facilitated, and the lower electrical resistance can be better attributed to electronic charge motion rather than any preferred ionic motion that may develop at the fiber-cement interface.

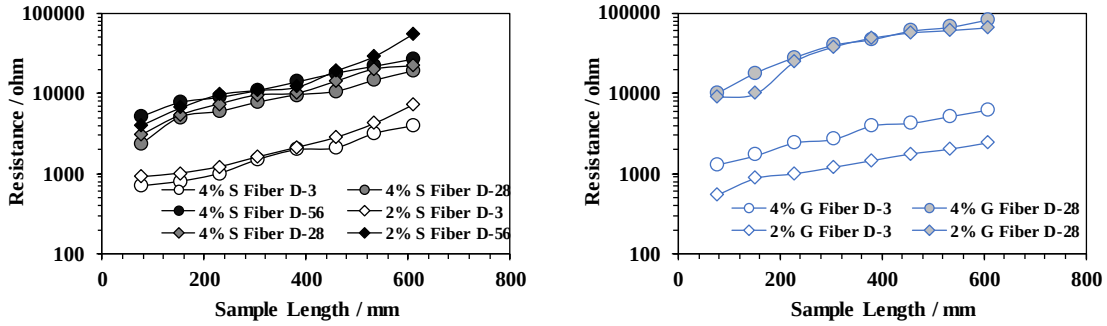

(a) (b)

Figure 17. Bulk Resistance of Specimens cast with (a) steel Fiber and (b) Glassfiber.

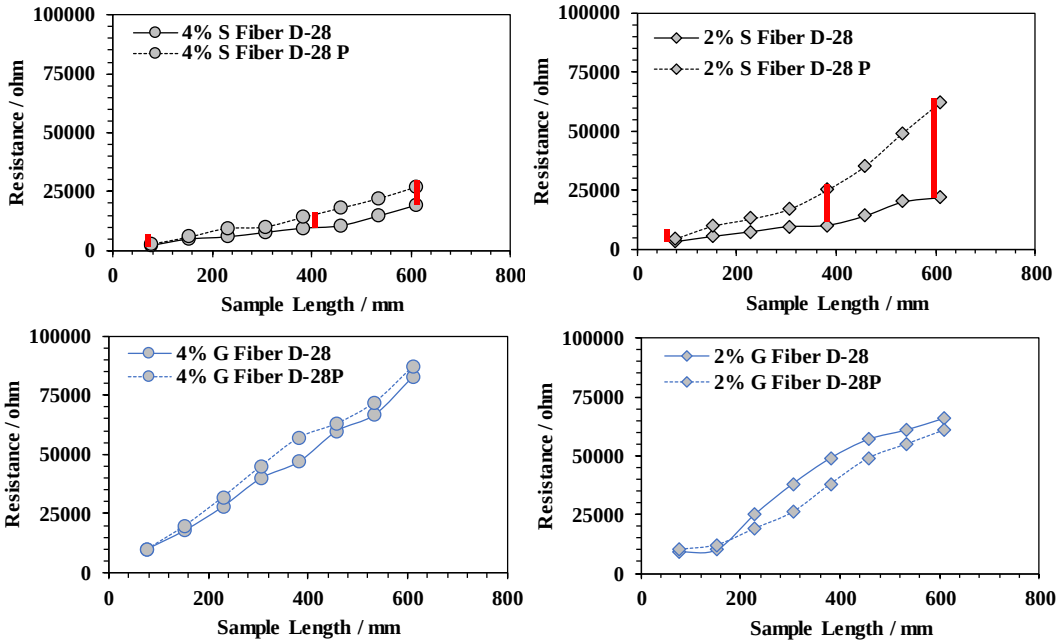

Figure 18. Difference in Bulk Resistance Due to Fiber Orientation. P represents alignment of the concrete sections with fibers perpendicular to the current path.

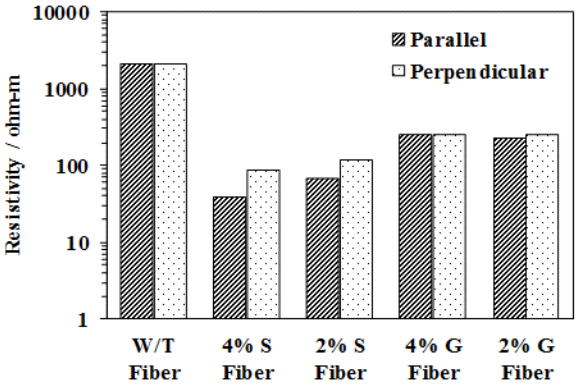

Figure 19. The difference in Resistivity Due to Fiber Property.

Figure 20 shows the results of EIS testing in the form of Nyquist diagrams. The impedance measurements were taken for all of the specimens with the working and counter electrodes configured such that the applied current flow lines are parallel or perpendicular to the fiber alignment. As expected, the Nyquist diagrams all showed two separate impedance loops representing a high frequency arc associated with the electrical response of the concrete and a low frequency arc associated with the interfacial characteristics of the steel electrodes.

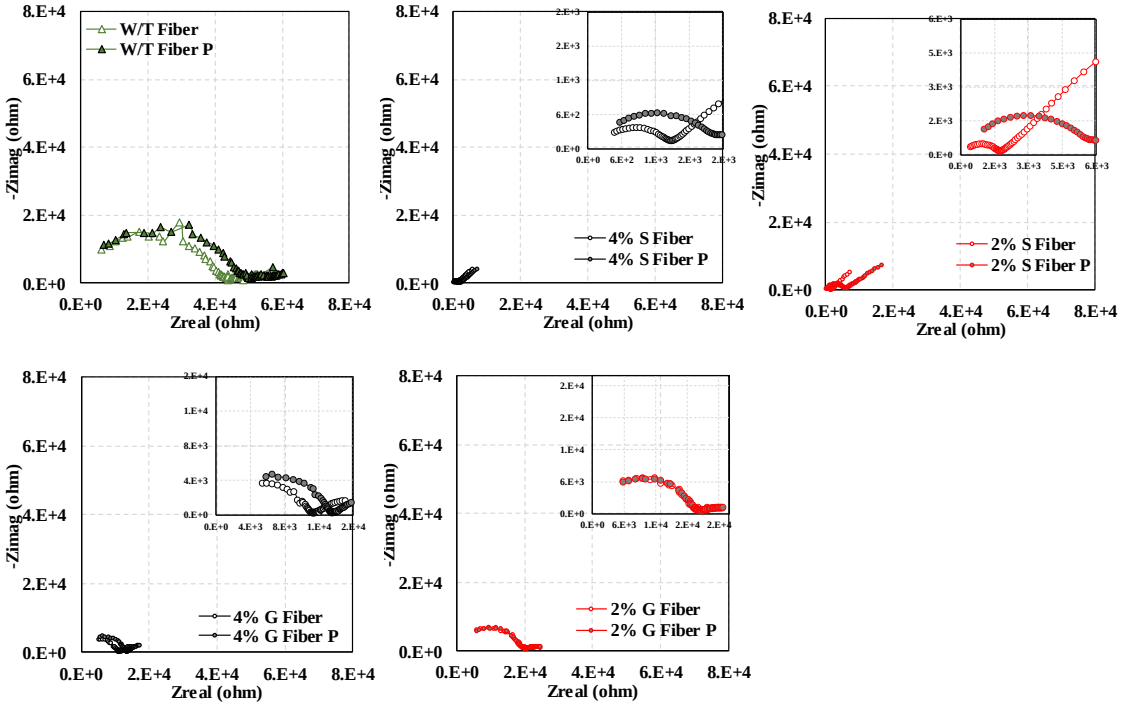

Figure 20. Nyquist Diagram of the UHPC Samples with Different Percentage of Fiber. (P represents data perpendicular to the casting direction)

The high frequency loop is associated with the dielectric property of the cementitious materials and the electrical resistance of bulk material. The control specimens without any fiber content showed a larger high frequency loop than the specimens with either steel or fiberglass fibers, characterizing the low permeability concrete. The high frequency loop was smaller in presence of either fibers. Of note, the orientation of the fibers only had significant influence on the impedance characteristics for the steel fiber UHPC where the high frequency loop was larger for the cases where the steel fibers were oriented perpendicular to the current flow line in comparison to where the steel fibers were oriented in parallel with the current flow lines.

Figure 21 shows the results of the concrete pore resistance resolved from equivalent circuit fitting of the high frequency impedance loop. General trends obtained by the electrical resistance measurement were observed by EIS. The smaller pore resistance of the specimens with fibers than without fibers was apparently due to the connected pore network in the UHPC matrix. The pore resistance was as expected lower with the greater fiber content. The comparatively smaller resistance of the UHPC with steel fiber than glass fiber was apparently due to the conductive and stiff nature of the steel fibers, which facilitates the connectivity of the internal capillary pores.

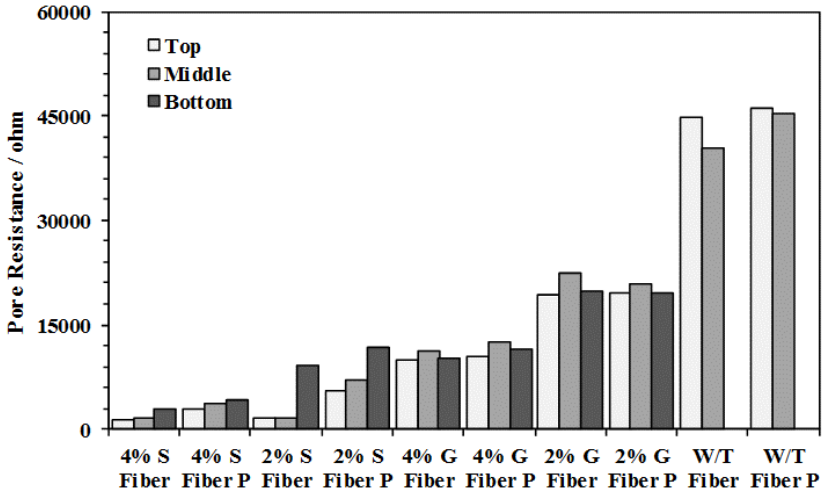

Figure 21. Pore resistance of the specimens measured by EIS

The result showed that the method of casting can have a significant influence on fiber distribution and orientation. This fiber orientation can have an important role in the movement of electrical and ionic charge through the UHPC bulk. The results showed that as the length of the UHPC sample increased, the resistivity of the UHPC bulk increased approximately linearly conforming to Ohm's law. The reason for not having a perfect linear correlation can be explained by having a non-uniform distribution of fibers in the length of specimens. The results showed that the resistivity of the UHPC increased significantly with concrete hydration as the ongoing hydration process and pozzolanic reactions that block the ionic path continues [47-50].

It was shown that by increasing the steel fiber content, the resistivity of bulk decreasing proportionally compared to the no-fiber control specimen. In the presence of the conductive steel fibers, electrical current was apparently facilitated. It was proposed that the presence of the conductive fibers can facilitate shorter paths for charged species to move in UHPC bulk by bridging ionic paths through the pores by electronic paths via the conductive fiber as illustrated in Figure 22 [47]. Sufficient concentration of fibers oriented in parallel to the current direction can provide more effective transport of charge and result is lower bulk resistivity. Furthermore, as shown by the decrease in resistance for the fiberglass laden specimens in comparison to the control fiber-less specimens, hydration of the cementitious materials at the interface of the solid fiber materials can create rich regions of cement paste that can favor ionic transport of chemical species through it gel pores.

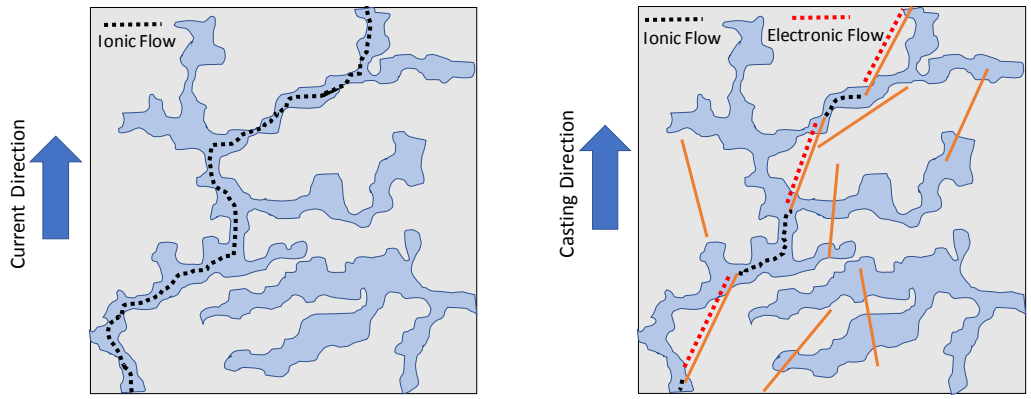

(a) (b)

Figure 22 Current flow between UHPC pores:(a) UHPC without fiber, (b) UHPC with fibers

These observations should require further exploration to address possible adverse effects of oriented fibers in UHPC on its electrical properties and in relation to macrocell coupling of reinforcing steel in UHPC retrofit. Furthermore, these results would suggest that characterizing the durability of UHPC by testing involving its electrical properties and migration of charged species should require further scrutiny.

4. SUMMARY OF RESULTS

Corrosion Behavior of Steel in UHPC Retrofitted T-Beam

- The steel embedded in the chloride contaminated region of the concrete T-beam developed highly electronegative potentials indicative of the expected corrosion activity. The electrical potentials of the rebar embedded in the chloride-free NC developed moderate potentials in the range of -0.2 to -0.4 V_{CSE} even though passive corrosion conditions was expected there. All of the rebar embedded in the UHPC developed passive potentials.

- The moderate potentials developed in the chloride-free NC concrete was related to the coupling of the actively corroding steel in the chloride-contaminated region. There can be significant polarization of the adjacent steel embedded in the rather poor quality concrete (lower resistivity). Conversely, this polarization did not occur for any of the steel rebar embedded in the UHPC (including those directly adjacent to the NC region. This observation highlights the effect of the high quality UHPC to minimize the extent of macrocell coupling of the anodes to the extended cathodes in the steel embedded in the shell repair.

- At day 36, there was a clear linear relationship between the macrocell current and the cathode-to-anode ratio for the cathodes in the UHPC repair. The larger extended cathode in the UHPC allowed for larger macrocell currents to develop. The macrocell current was much larger when the cathode was the steel embedded in the concrete core substrate. Even though the embedded steel there would be encapsulated with the UHPC that could minimize oxygen transport, there would be sufficient oxygen in the substrate concrete pore water to support the cathodic oxygen reduction reaction.

Effect of Fibers on UHPC Electrical Behavior

- The method of casting can have a significant influence on fiber distribution and orientation. The electrical resistance for all materials was lower with the shorter specimen lengths due to the shorter path for charge to travel and lower at the

earlier hydration time (and shorter exposure in the 100%RH chamber) due to the shorter time for the clinker to hydrate and the shorter time for moisture penetration from the conditioning environment. Specimens with 2% steel fiber showed slightly higher resistance than samples with steel 4% fiber.

- The results show that the presence of fibers have an effect to reduce the overall electrical resistivity likely in part related to partial volume replacement of high quality cement and possibly oriented pathways in the cement microstructure along the fiber interface that can facilitate ionic movement. The results suggested that the parallel orientation of conductive fibers with the current path at high enough concentrations can create a system where electronic charge through the conductive fiber can be facilitated, and the lower electrical resistance can be better attributed to electronic charge motion rather than any preferred ionic motion that may develop at the fiber-cement interface.

- The orientation of the steel fibers have significant influence on the overall bulk UHPC resistance. Specimens with the steel fiber aligned orthogonal to the current path resulted in larger electrical resistance in comparison to when the steel fibers were aligned parallel with the current path. This effect was not observed for the specimens cast with fiberglass. Also, the overall electrical resistance was lower for the specimens cast with steel fibers than the less conductive fiberglass fibers.

- It was proposed that the presence of the conductive fibers can facilitate shorter paths for charged species to move in UHPC bulk by bridging ionic paths through the pores by electronic paths via the conductive fiber

REFERENCES

[1] Koch, G.H., Brongers, M.P.H., Thompson, T.G., Virmani, Y.P., and Payer, J.H. “Corrosion Costs and Preventive Strategies in the Unites States.” Publication No. FHWA-RD-01-156.

[2] AP News. “Repairs close lanes on weekends of I-526 Wando River bridges.”June 2, 2019. Retrieved from https://apnews.com/article/7206e61a3334476487da6988e422eb3e on March 16, 2021

[3] Farzad, M., Garber, G., Azizinamini, A., and Lau, K. “Corrosion Macrocell Development in Reinforced Concrete with Repair UHPC. NACE Corrosion/2018. Paper No. 11580. Houston, Nace International 2018.

[4] Farzad, M., Fancy., S.F., Lau, K., and Azizinamini, A. “Chloride Penetration at Cold Joints of Structural Members with Dissimilar Concrete Incorporating UHPC. Infrastructures. V.4, No. 2, 18. **https://doi.org/10.3390/infrastructures4020018**

[5] Graybeal BA. Material property characterization of ultra-high performance concrete. United States. Federal Highway Administration. Office of Infrastructure Research and Development; 2006 Aug 1.

[6] Russell HG, Graybeal BA, Russell HG. Ultra-high performance concrete: A state-of-the-art report for the bridge community. United States. Federal Highway Administration. Office of Infrastructure Research and Development; 2013 Jun 1.

[7] de Larrard F, Sedran T. Optimization of ultra-high-performance concrete by the use of a packing model. Cement and concrete research. 1994 Jan 1;24(6):997-1009.

[8] Graybeal, Benjamin. "Ultra-High Performance Concrete (FHWA-HRT-11-038)." *Federal Highway Administration, Washington, DC* (Mar,2011).

[9] Richard P, Cheyrezy M. Composition of reactive powder concretes. Cement and concrete research. 1995 Oct 1;25(7):1501-11.

[10] Schmidt M, Fehling E. Ultra-high-performance concrete: research, development and application in Europe. ACI Special publication. 2005 Jun 1;228:51-78.

[11] Ghafari E, Costa H, Júlio E. Critical review on eco-efficient ultra high performance concrete enhanced with nano-materials. Construction and Building Materials.

2015 Dec 30;101:201-8.

[12] Vernet, Christian P. "Ultra-durable concretes: structure at the micro-and nanoscale." *MRS bulletin* 29, no. 5 (May,2004): 324-327.

[13] Wille, Kay, Antoine E. Naaman, and Gustavo J. Parra-Montesinos. "Ultra-High Performance Concrete with Compressive Strength Exceeding 150 MPa (22 ksi): A Simpler Way." *ACI materials journal* 108, no. 1 (Jan,2011).

[14] Shi, Caijun, Zemei Wu, Jianfan Xiao, Dehui Wang, Zhengyu Huang, and Zhi Fang. "A review on ultra high performance concrete: Part I. Raw materials and mixture design." *Construction and Building Materials* 101 (Dec,2015): 741-751.

[15] Abbas, Safeer, Ahmed M. Soliman, and Moncef L. Nehdi. "Exploring mechanical and durability properties of ultra-high performance concrete incorporating various steel fiber lengths and dosages." *Construction and Building Materials* 75 (Jan,2015): 429-441.

[16] Schmidt M, Fehling E, Geisenhanslüke C. Ultra high performance concrete (UHPC). InProceedings of the international symposium on ultra High Performance Concrete, Kassel, germany. university of Kassel, germany 2004 Sep 13.

[17] Talebinejad, Iman, Seyed Asadollah Bassam, Amirhossein Iranmanesh, and Mohammad Shekarchizadeh. "Optimizing mix proportions of normal weight reactive powder concrete with strengths of 200–350 MPa." In *Proceedings of the International Symposium on UHPC, Kassel, Germany*, pp. 133-141. Sep,2004.

[18] Ghoddousi, Parviz, Armin Monir Abbasi, Esmail Shahrokhinasab, and Mohammad Abedin. "Prediction of Plastic Shrinkage Cracking of Self-Compacting Concrete." *Advances in Civil Engineering* 2019.pp. 1–7, Oct. 2019.

[19] Yazıcı, Halit. "The effect of curing conditions on compressive strength of ultra high strength concrete with high volume mineral admixtures." *Building and environment* 42, no. 5 (May,2007): 2083-2089.

[20] Abbas, S., M. L. Nehdi, and M. A. Saleem. "Ultra-high performance concrete: Mechanical performance, durability, sustainability and implementation challenges." *International Journal of Concrete Structures and Materials* 10, no. 3 (Sep,2016): 271-295.

[21] Nicolaides D, Kanellopoulos A, Petrou MF, Soutsos M. Mix design, mechanical

properties and impact resistance of UHPFRCCs. InProceedings of the 3 rd International Conference on Concrete Repair, Rehabilitation and Retrofitting, ICCRRR-3, Alexander, MG 2012 Oct 17 (pp. 181-186).

[22] Gao, Ri, Zhi Min Liu, Li Qian Zhang, and Piet Stroeven. "Static properties of plain reactive powder concrete beams." In *Key Engineering Materials*, vol. 302, pp. 521-527. Trans Tech Publications Ltd, 2006.

[23] Wen-yu, Ji, An Ming-zhe, Yan Gui-ping, and Wang Jun-min. "Study on reactive powder concrete used in the sidewalk system of the Qinghai-Tibet railway bridge." In *International Workshop on Sustainable Development and Concrete Technology, Beijing, China*, pp. 333-338. May,2004.

[24] Rougeau, Patrick, and Béatrice Borys. "Ultra high performance concrete with ultrafine particles other than silica fume." In *Proceedings of the International Symposium on Ultra High Performance Concrete*, vol. 32, pp. 213-225. Sep,2004.

[25] Tue, Nguyen Viet, Jianxin Ma, and Marko Orgass. "Influence of addition method of superplasticizer on the properties of fresh UHPC." In *Proceedings of the 2nd International Symposium on Ultra-High Performance Concrete, Kassel, Germany*, pp. 93-100.March,2008.

[26] E. Fehling, M. Schmidt, and S. Stürwald, *Ultra High Performance Concrete (UHPC): Proceedings of the Second International Symposium on Ultra High Performance Concrete, Kassel, Germany*. 2008.

[27] Droll K. Influence of additions on ultra high performance concretes–grain size optimisation. InProceedings of the International Symposium on UHPC, Kassel, Germany 2004 Sep 13 (pp. 285-301).

[28] Teichmann, Thomas, and Michael Schmidt. "Influence of the packing density of fine particles on structure, strength and durability of UHPC." In *International symposium on ultra high performance concrete*, pp. 313-323. 2004.

[29] Teichmann, Thomas, and Michael Schmidt. "Influence of the packing density of fine particles on structure, strength and durability of UHPC." In *International symposium on ultra high performance concrete*, pp. 313-323. Sep 13,2004.

[30] Ahlborn, Theresa (Tess) M., Devin K. Harris, Donald L. Misson, and Erron J. Peuse. "Characterization of strength and durability of ultra-high-performance

concrete under variable curing conditions." *Transportation research record* 2251, no. 1 (2011): 68-75.

[31] ASTM International. *C1202-19 Standard Test Method for Electrical Indication of Concrete's Ability to Resist Chloride Ion Penetration*. West Conshohocken, PA; ASTM International, 2019. doi: https://doi.org/10.1520/C1202-19

[32] Foudazi A, Mehdipour I, Donnell KM, Khayat KH. Evaluation of steel fiber distribution in cement-based mortars using active microwave thermography. Materials and Structures. 2016 Dec 1;49(12):5051-65.

[33] Bayard O, Plé O. Fracture mechanics of reactive powder concrete: material modelling and experimental investigations. Engineering fracture mechanics. 2003 May 1;70(7-8):839-51.

[34] Kang, Su Tae, Bang Yeon Lee, Jin-Keun Kim, and Yun Yong Kim. "The effect of fibre distribution characteristics on the flexural strength of steel fibre-reinforced ultra high strength concrete." *Construction and Building Materials* 25, no. 5 (May 1,2011): 2450-2457.

[35] Torrijos, María C., Bryan E. Barragán, and Raúl L. Zerbino. "Placing conditions, mesostructural characteristics and post-cracking response of fibre reinforced self-compacting concretes." *Construction and Building Materials* 24, no. 6 (Jun 1,2010): 1078-1085.

[36] Emdadi, Arezoo, Iman Mehdipour, Nicolas Ali Libre, and Mohammad Shekarchi. "Optimized workability and mechanical properties of FRCM by using fiber factor approach: theoretical and experimental study." *Materials and Structures* 48, no. 4 (Apr 1,2015): 1149-1161.

[37] Ferrara, Liberato, Nilufer Ozyurt, and Marco Di Prisco. "High mechanical performance of fibre reinforced cementitious composites: the role of "casting-flow induced" fibre orientation." *Materials and Structures* 44, no. 1 (Jan 1,2011): 109-128.

[38] Foudazi, Ali, Iman Mehdipour, Kristen M. Donnell, and Kamal H. Khayat. "Evaluation of steel fiber distribution in cement-based mortars using active microwave thermography." *Materials and Structures* 49, no. 12 (2016): 5051-5065

[39] Zhou, Jian, Shunzhi Qian, Guang Ye, Oguzhan Copuroglu, Klaas van Breugel,

and Victor C. Li. "Improved fiber distribution and mechanical properties of engineered cementitious composites by adjusting the mixing sequence." *Cement and Concrete Composites* 34, no. 3 (March 1,2012): 342-348.

[40] Akcay, Burcu, and Mehmet Ali Tasdemir. "Mechanical behaviour and fibre dispersion of hybrid steel fibre reinforced self-compacting concrete." *Construction and Building Materials* 28, no. 1 (March 1, 2012): 287-293.

[41] Ujan, Sahar, Seyed Ghorshi, Majid Pourebrahim, and Seyed Alireza Khoshnevis. "On the use of compressive sensing for image enhancement." In *2016 UKSim-AMSS 18th International Conference on Computer Modelling and Simulation (UKSim)*, pp. 167-171. IEEE, Apr 6,2016.

[42] Zelelew, H. M., A. T. Papagiannakis, and E. Masad. "Application of digital image processing techniques for asphalt concrete mixture images." In *The 12th International Conference of International Association for Computer Methods and Advances in Geomechanics (IACMAG)*, pp. 119-124. Oct 1,2008.

[43] Meng, Weina, and Kamal Henri Khayat. "Improving flexural performance of ultra-high-performance concrete by rheology control of suspending mortar." *Composites Part B: Engineering* 117 (May 15,2017): 26-34.

[44] Knight, Marcus L., G. Scott Wilson, Wayne J. Seger, and Sankaran Mahadevan. "Overlay types used as preventive maintenance on Tennessee bridge decks." *Transportation research record* 1866, no. 1 (May,2004): 79-84.

[45] Gettu, R., Diane Ruth Gardner, H. Saldivar, and B. E. Barragán. "Study of the distribution and orientation of fibers in SFRC specimens." *Materials and Structures* 38, no. 1 (Jan 1,2005): 31-37.

[46] Naaman, A. E., and K. Wille. "Some correlation between high packing density, ultra-high performance, flow ability, and fiber reinforcement of a concrete matrix." *BAC2010—2nd Iber Congr Self Compact* (July 1,2010).

[47] Fan, Liang, Weina Meng, Le Teng, and Kamal Henri Khayat. "Effect of steel fibers with galvanized coatings on corrosion of steel bars embedded in UHPC." *Composites Part B: Engineering* 177 (Nov 15,2019): 107445.

[48] Montemor, M. F., A. M. P. Simoes, and M. M. Salta. "Effect of fly ash on concrete reinforcement corrosion studied by EIS." *Cement and Concrete Composites* 22,

no. 3 (Jun 1,2000): 175-185.

[49] Dotto, J. M. R., A. G. De Abreu, D. C. C. Dal Molin, and I. L. Müller. "Influence of silica fume addition on concretes physical properties and on corrosion behaviour of reinforcement bars." *Cement and concrete composites* 26, no. 1 (Jan 1,2004): 31-39

[50] Ma, Hongyan, Dongshuai Hou, and Zongjin Li. "Two-scale modeling of transport properties of cement paste: Formation factor, electrical conductivity and chloride diffusivity." *Computational Materials Science* 110 (Dec 1,2015): 270-280.